

Bulking up: hexanuclear oximato Fe(III) complexes surrounded by sterically demanding co-ligands

Item Type	Journal article
Authors	Houton, E;Meally, ST;Sanz, S;Brechin, EK;Jones, Leigh
Citation	Houton, E., Meally, S. T., Sanz, S., Brechin, E. K., Jones, L. F. (2014) Bulking up: hexanuclear oximato fe(iii) complexes surrounded by sterically demanding co-ligands. <i>Inorganica Chimica Acta</i> 421, pp. 416-422.
DOI	10.1016/j.ica.2014.06.021
Publisher	Elsevier
Journal	<i>Inorganica Chimica Acta</i>
Download date	2026-06-07 01:24:08
License	https://creativecommons.org/licenses/by-nc-nd/4.0/
Link to Item	http://hdl.handle.net/2436/623020

Bulking Up: Hexanuclear Oximate Fe(III) Complexes Surrounded by Sterically Demanding Co-Ligands

Edel Houton,^a Sean T. Meally,^a Sergio Sanz,^b Euan K. Brechin^b and Leigh F. Jones.^{a,*‡}

[‡] Current address: School of Chemistry, Bangor University, Bangor, Wales. LL57 2DG. Tel: +44-(0)1248-38-2391. Email: leigh.jones@bangor.ac.uk

^a School of Chemistry, NUI Galway, University Road, Galway, Ireland.

^b EaStCHEM School of Chemistry, University of Edinburgh, West Mains Road, Edinburgh, EH9 3JJ, Scotland.

Abstract

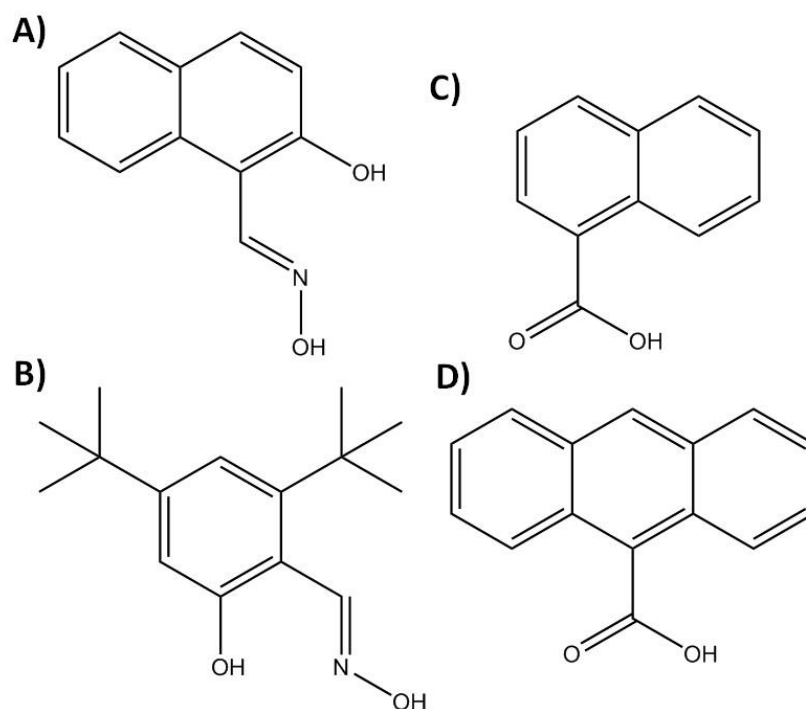
Despite their inherent steric bulk, a combination of 2-hydroxy-1-naphthaldoxime (L_1H_2) with polyphenolic carboxylate ligands (1-Naphthoate, 9-Anthracene carboxylate) aid the construction and stabilisation of hexanuclear arrays of Fe(III) ions in the form of $[Fe(III)_6O_2(L_1)_2(O_2C-R)_{10}(H_2O)_2] \cdot 8MeCN$ ($R = Naphth-$ ($C_{10}H_8$) (**1**); $R = Anthra-$ ($C_{14}H_9$) (**2**)). Likewise, the sterically hindered ligand 3,5-di-tert-butyl-salicylaldoxime (L_2H_2) is able to aid the self-assembly of the tetranuclear, cubane-like species $[Fe(III)_4(L_2)_4(MeOH)_4(Cl)_4]$ (**3**). Magnetic susceptibility studies carried out on **1** and **3** reveal antiferromagnetic exchange between the Fe(III) metal centres affording $S = 0$ ground spin states in both cases.

1. Introduction

Functionalised phenolic oximes have extensive application as ligands in the solvent extraction of copper, accounting for *ca.* 25% of worldwide production [1]. Complex stability upon binding is (at least in part) due to the formation of pseudo macrocyclic $[Cu(L)_2]$ (where $L =$ phenolic oxime) moieties. Recent studies by Forgan *et al* have shown that extractant strength may be tuned by controlling the extent of outer sphere H-bonding interactions [2]. Although exhibiting a great affinity towards copper, oximes have also formed many interesting [often polymetallic] coordination complexes with other 1st row transition metals [3,4]. A good example is the use of derivatised salicylaldoximes (R -saoH₂; $R = H, Me, Et, Ph, ^tBu$ *etc*) in the formation of a large family of $[Mn_3]$ and $[Mn_6]$ Single-Molecule Magnets (SMMs) [5]. Moreover it was shown inextricably that the ground spin states of these magnetic cages could be tuned and controlled by modification of the bridging salicylaldoxime ligands at their R positions [6]. Although $[Mn_3]$ and $[Mn_6]$ cage formation was found to be

predictable and under near complete synthetic control, investigations into the coordination chemistry of the same salicyldoximes with iron has proven to be far more difficult and less predictable, giving rise to ferric cages of numerous sizes (ranging from $\{\text{Fe}_2\}$ [7] to $\{\text{Fe}_{12}\}$ [8]) and topologies, depending on specific synthetic factors, such as the type of oxime, the nature of the co-ligand (*e.g.* carboxylate), solvent identity, and temperature/pressure [9b].

With these thoughts in mind we decided to examine the role of sterically demanding oximes and carboxylate co-ligands towards Fe-oxime cage formation [10] and quickly settled on investigating combinations of 2-hydroxy-1-naphthaldoxime (L_1H_2 ; Scheme 1) and the carboxylate anions 1-Naphthoate (${}^{-}\text{O}_2\text{-C-C}_{10}\text{H}_8$) and 9-Anthracenecarboxylate (${}^{-}\text{O}_2\text{C-C}_{12}\text{H}_{10}$) (Scheme 1). To this end we present the hexametallc siblings $[\text{Fe}(\text{III})_6\text{O}_2(\text{L}_1)_2(\text{O}_2\text{C-C}_{10}\text{H}_8)_{10}(\text{H}_2\text{O})_2] \cdot 8\text{MeCN}$ (**1**) and $[\text{Fe}(\text{III})_6\text{O}_2(\text{L}_1)_2(\text{O}_2\text{C-C}_{14}\text{H}_{10})_{10}(\text{H}_2\text{O})_2] \cdot 8\text{MeCN}$ (**2**), and the tetranuclear cube-like cage $[\text{Fe}(\text{III})_4(\text{L}_2)_4(\text{MeOH})_4(\text{Cl})_4]$ (**3**) constructed using 3,5-di-*tert*-butyl salicyldoxime (L_2H_2 , Scheme 1).



Scheme 1: ChemDraw representations of the ligands 2-hydroxy-1-naphthaldoxime (L_1H_2 ; **A**), 3,5-di-*tert*-butyl-salicyldoxime (L_2H_2 ; **B**), 1-Naphthoic acid (**C**) and 9-Anthracene carboxylic acid (**D**).

2. Experimental Section

2.1 Materials and physical measurements

Infra-red spectra were recorded on a Perkin Elmer FT-IR *Spectrum One* spectrometer equipped with a Universal ATR Sampling accessory (NUI Galway). Elemental analysis was carried at the School of Chemistry microanalysis service at NUI Galway. Variable-temperature, solid-state direct current (dc) magnetic susceptibility data down to 1.8 K were collected on a Quantum Design MPMS-XL SQUID magnetometer equipped with a 7 T dc magnet. Diamagnetic corrections were applied to the observed paramagnetic susceptibilities using Pascal's constants.

2.2 Crystal structure information

Complexes **1-3** were collected on an Xcalibur S single crystal diffractometer (Oxford Diffraction) using an enhanced Mo source (CCDC numbers: 999462 (**1**), 999463 (**2**) and 999461 (**3**)). Each data reduction was carried out on the CrysAlisPro software package. The structures were solved by direct methods (SHELXS-97) [11] and refined by full matrix least squares using SHELXL-97 [12]. SHELX operations were automated using the OSCAIL software package.[13] All hydrogen atoms in **1-3** were assigned to calculated positions. All non-hydrogen atoms were refined as anisotropic. A DFIX restraint was placed on a single MeCN solvent of crystallisation in **2** (labelled C93-C94-N5). Crystal data and refinement parameters are tabulated in Table 1. Single crystals of complex **2** were found to be weakly diffracting at higher angles and therefore several collections were attempted. Our best data set has been supplied in this work ($R_1 = 0.1285$).

2.3 Synthetic Details

All reactions were performed under aerobic conditions and all reagents and solvents were used as purchased. Ligands L_1H_2 and L_2H_2 were synthesised using literature methods [14].

2.3.1 Synthesis of $[Fe(III)_6O_2(L_1)_2(O_2C-C_{10}H_8)_{10}(H_2O)_2] \cdot 8MeCN$ (**1**)

$FeCl_2 \cdot 4H_2O$ (0.25 g, 1.26 mmol), L_1H_2 (0.235 g, 1.26 mmol), Sodium 1-Naphthoate (0.242 g, 1.25 mmol) and NaOMe (0.068 g, 1.26 mmol) were stirred in MeOH (30 cm³) for 2 h, filtered and allowed to evaporate to dryness. The resultant solid was dissolved in a 1:1 MeCN:CH₂Cl₂ solvent mixture, filtered and left to stand. Dark red crystals of **1** were formed upon slow evaporation in 20% yield over a period of 5 days. Elemental analysis (%) calculated (found) for C₁₄₈H₁₁₂N₁₀O₂₈Fe₆: C 63.18 (63.37), H 4.01 (3.84); N 4.98 (4.55). FT-IR (cm⁻¹): 3051(w), 1617(w), 1597(w), 1578(w), 1541(m), 1525(m), 1509 (m), 1459(w),

1408(s), 1375(s), 1343(vs), 1257(m), 1209 (w), 1184(w), 1157(w), 1139(w), 1077(w), 1037(w), 1010(w), 998(w), 941(m), 870(vw), 826(w), 782(vs), 757(m), 750(m), 672(w).

2.3.2 Synthesis of $[Fe(III)_6O_2(L_1)_2(O_2C-C_{14}H_{10})_{10}(H_2O)_2] \cdot 8MeCN$ (**2**)

$FeCl_2 \cdot 4H_2O$ (0.25 g, 1.26 mmol), L_1H_2 (0.235 g, 1.26 mmol), Sodium 9-Anthracene carboxylate (0.307 g, 1.26 mmol) and NaOH (0.05 g, 1.25 mmol) were stirred in EtOH (30 cm³) for 2 h, filtered and allowed to evaporate to dryness. The resultant solid was then dissolved in a 1:1 MeCN:CH₂Cl₂ solvent mixture, filtered and left to stand. Dark red crystals of **2** were formed upon slow evaporation in 15% yield after 5 days. Elemental analysis (%) calculated (found) for C₁₈₈H₁₃₂N₁₀O₂₈Fe₆: C 68.13 (68.37), H 4.01 (3.84); N 4.23 (4.11). FT-IR (cm⁻¹): 2982(vb), 1616(w), 1555(s), 1529(m), 1487 (w), 1425(s), 1391(s), 1317(s), 1279(m), 1248(w), 1187(w), 1143(w), 1092(w), 1034(w), 1014(m), 954(m), 884(w), 866.2(w), 846(w), 825(w), 782(w), 729(s), 679(m), 662(m).

2.3.3 Synthesis of $[Fe(III)_4(L_2)_4(MeOH)_4(Cl)_4]$ (**3**).

To a stirring solution of $FeCl_2 \cdot 4H_2O$ (0.25 g, 1.26 mmol) in MeOH (25 cm³) was added 3,5-di-*tert*-butyl-salicylaldoxime (0.313 g, 1.26 mmol) and NaOH (0.05 g, 1.26 mmol). The solution was stirred for 2 h after which time it was filtered to afford a purple-black mother liquor. Slow evaporation of the solvent afforded X-ray quality crystals of **3** in 45% yield. Elemental Analysis calculated (found) for **3** (C₆₄H₁₀₀N₄Cl₄Fe₄O₁₂): C 51.87 (51.42); H 6.80 (6.54); N 3.78 (3.30). FT-IR (cm⁻¹): 3243(w), 2956(m), 2905(w), 2869(w), 1602(w), 1586(m), 1548(w), 1534(w), 1478(w), 1460(w), 1423(m), 1387(w), 1363(m), 1296(m), 1273(m), 1253(s), 1232(w), 1201(m), 1174(m), 1136(w), 1118(w), 1005(m), 973(s), 954(s), 930(w), 902(w), 874(w), 842(s), 817(w), 775(m), 749(m), 711(s).

3. Results and Discussion

The reaction of $FeCl_2 \cdot 4H_2O$, L_1H_2 , Sodium 1-Naphthoate and NaOMe in MeOH resulted in the formation of a black solid after evaporation of the mother liquor. Subsequent dissolution of this solid in a 50:50 MeCN:CH₂Cl₂ solvent mixture, followed by filtration and slow evaporation of the mother liquor afforded dark red crystals of $[Fe(III)_6O_2(L_1)_2(O_2C-C_{10}H_8)_{10}(H_2O)_2] \cdot 8MeCN$ (**1**) in 20% yield. As anticipated, employing Sodium 9-Anthracenecarboxylate gave rise to the analogous hexanuclear complex $[Fe(III)_6O_2(L_1)_2(O_2C-C_{14}H_{10})_{10}(H_2O)_2] \cdot 8MeCN$ (**2**) in 15% yield. Complexes **1** and **2** both

crystallise in the triclinic *P*-1 space group. Their inorganic cores consist of two fused [Fe(III)₃(μ₃-O)(O₂-CR)₅] triangular units (where R = C₁₀H₈ in **1**; R = C₁₄H₁₀ in **2**), lying offset to one another (Fig. 1 and S1). Complexes **1** and **2** join a small group of previously reported oxime-based hexametallc cages which include [Fe₆O₂(O₂CPh)₁₀(salox)₂] (salox = salicyldoxime) [9a] and [Fe₆O₂(O₂CPh)₁₀(R-sao)₂] (R-saoH₂ = 3-^tBu-5-NO₂-salicyldoxime and 3-^tBu-salicyldoxime) [9b]. They also have structural similarity to another family of hexanuclear cages of general formula [Fe₆O₂(OH)₂(O₂C-R)₁₀(L)₂] (R = ^tBu, L = 2-(2-hydroxyethyl)-pyridine [15]; and R = ^tBu or Me, L = 2-(2-hydroxyethyl)-pyridine or 6-methyl-2-(hydroxymethyl)pyridine [16]), whose inorganic cores differ only in the presence of two μ₂-bridging OH⁻ anions [17].

Each Fe(III) centre exhibits a distorted octahedral geometry. The triangular units in **1** and **2** closely resemble the classic, ubiquitous oxo-bridged trimeric species of general formula [M₃(μ₃-O)(O₂-CR)₆(L)₃]ⁿ⁺ (n = 0, 1) [18], differing only in the replacement of one carboxylate bridging ligand with one L²⁻ ligand per {Fe₃(μ₃-O)(O₂-CR)₅}²⁺ unit. Indeed these η¹:η¹:η²:μ₃-bridging oxime ligands are responsible for joining the trimeric units together *via* their oximic O atoms (O2 in **1** and O3 in **2**) with angles of Fe3-O2-Fe3' = 104.48° and Fe3-O3-Fe3' = 106.49°, respectively. Moreover, each of these doubly deprotonated oxime ligands (L²⁻) are able to bridge one Fe^{III}-Fe edge of each {Fe₃(μ₃-O)} unit (Fe1^{III}-Fe3 in **1** and Fe2^{III}-Fe3 in **2**) to form Fe-N-O-Fe pathways (Fig. 1). The coordination spheres at Fe2 in **1** and Fe1 in **2** (and symmetry equivalents) are completed by terminal H₂O ligands (Fe2-O14 = 2.118 Å, Fe1-O14 = 2.103 Å). Eight MeCN solvents of crystallisation per Fe₆ cage are also present in both crystal structures, H-bonding *via* their N atoms to nearby carboxylate and H₂O ligands (*e.g.* C43(H43)⋯N5 = 2.690 Å and O14⋯N2 = 2.812 Å in **1**; C50(H50)⋯N2 = 2.671 Å and O14⋯N2 = 2.834 Å in **2**). Both complexes **1** and **2** exhibit intra-molecular π-π interactions *via* their naphthoate and anthracenoate rings, in the form of π-π contacts (*e.g.* [C₄₆-C₅₅]_{centroid}⋯[C₃₅-C₄₀]_{centroid} = 4.042 Å (**1**) and [C₁₃-C₂₆]⋯[C₅₈-C₇₁] = 3.988 Å (**2**)) (Fig. S2).

The individual {Fe₆} units in **1** arrange in superimposable 1-D rows along the *b* cell direction (Fig. 2). These rows stack on top and by the side of one another (along the *ac* plane) in an interdigitated fashion, propagated through C-H⋯π interactions between {Fe₆} moieties (*e.g.* C₉(H₉)⋯[C₁₄-C₁₉] = 2.934 Å) (Fig. 3). The MeCN molecules of crystallisation lie in between the cages in **1**, stabilising this packing arrangement through the aforementioned inter-molecular interactions.

The individual $\{\text{Fe}_6\}$ units in **2** arrange themselves into superimposable rows along the c cell direction and are linked *via* symmetry related inter-molecular π - π interactions ($[\text{C}_{29}\text{-C}_{34}]_{\text{centroid}} \cdots [\text{C}_{29'}\text{-C}_{34'}]_{\text{centroid}} = 3.842 \text{ \AA}$) (Fig. 2). These rows then stack in off-set parallel rows in both the a and b cell directions. MeCN molecules of crystallisation lie in between the 1-D rows and are held by hydrogen bonding, as described previously in **1**.

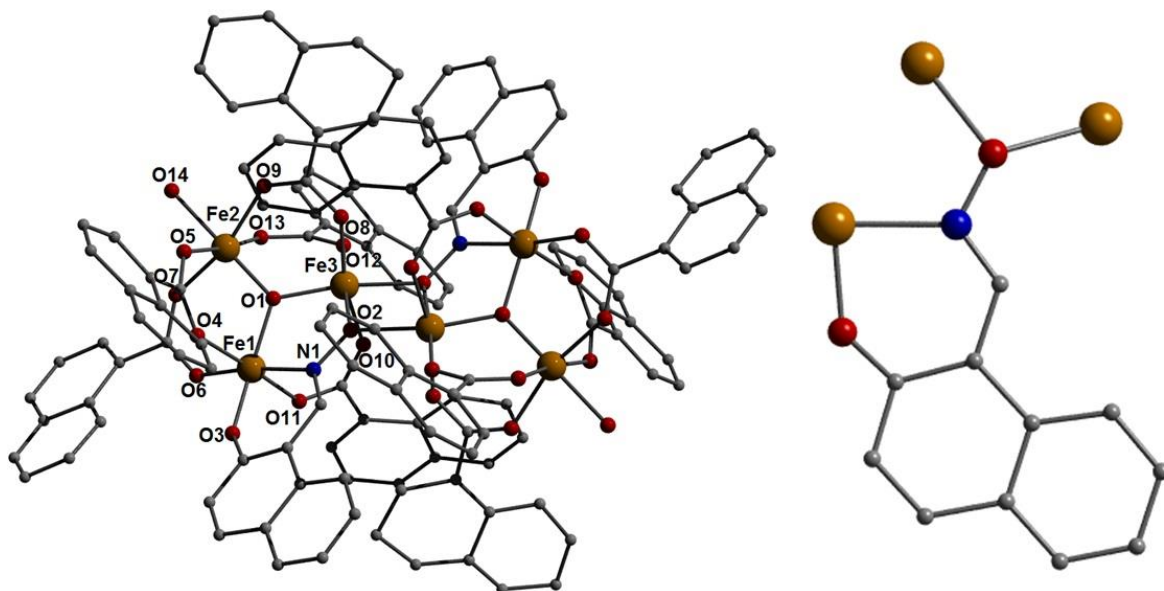


Figure 1 (left) Crystal structure of **1** as viewed perpendicular to the $\{\text{Fe}_6\}$ plane. (right) The $\eta^1:\eta^1:\eta^2:\mu_3$ -bonding mode demonstrated by the oxime ligands in **1** and **2**. Colour code: Orange (Fe), Red (O), Blue (N), Grey (C). Hydrogen atoms omitted for clarity.

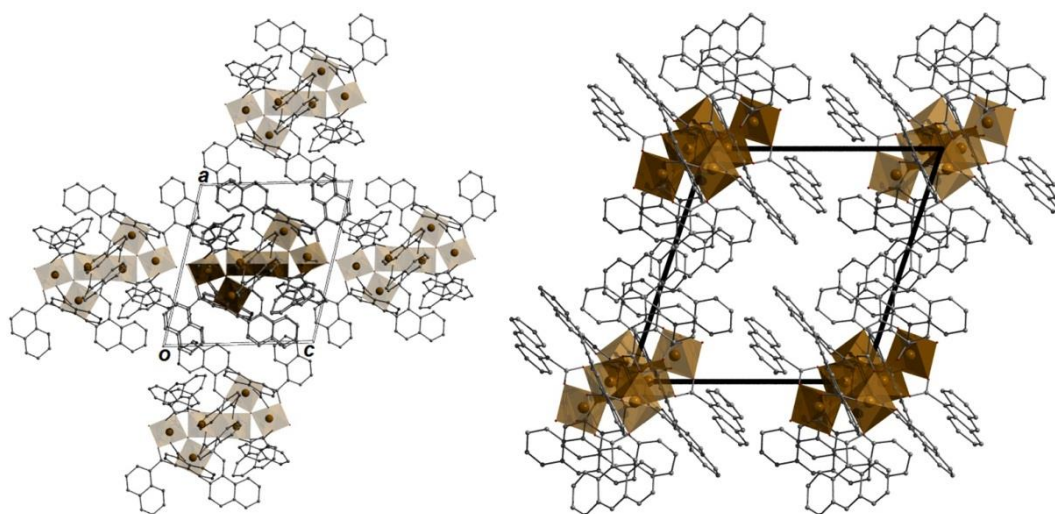


Figure 2 Polyhedral representation of the packing observed in the crystal structures of **1** (left) and **2** (right) as viewed along the *b* and *c* axes of their unit cells, respectively. Hydrogen atoms and MeCN molecules of crystallisation have been omitted for clarity in both cases.

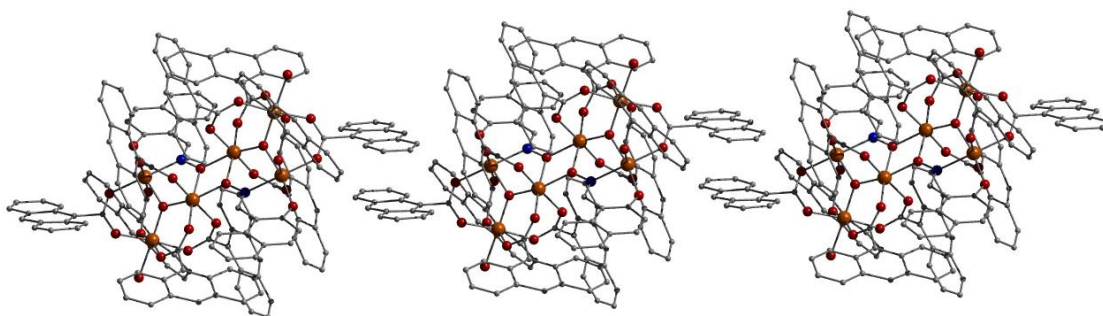


Figure 3 1-D row of {Fe₆} units in **2** propagated by inter-molecular π - π interactions along the *c* cell direction. Hydrogen atoms have been omitted for clarity. See main text for details.

Reactions of the rarely employed 3,5-di-*tert*-butyl-salicylaldoxime (L₂H₂; Scheme 1) in combination with bulky carboxylates proved fruitless, but omission of the co-ligand resulted in formation of [Fe(III)₄(L₂)₄(MeOH)₄(Cl)₄] (**3**) via the simple reaction of FeCl₃·4H₂O and L₂H₂ in a basic methanolic solution (Fig. 4). Dark red crystals of (**3**) were obtained in 45% yield and crystallised in the monoclinic space group *C2/c* (*Z* = 4). The inorganic core in **3** comprises four Fe(III) ions (Fe1, Fe2 and symmetry equivalents) linked into a distorted tetrahedral arrangement via four doubly deprotonated L₂²⁻ ligands, each employing an $\eta^1:\eta^1:\eta^2$: μ_3 -bonding motif (Fig. 4). The result is the formation of a severely distorted {Fe(III)₄(NO)₄}⁴⁺ cube, a topology observed only once previously in Fe-oxime chemistry [7]. Each Fe(III) ion exhibits a distorted octahedral geometry, with their coordination spheres completed by one Cl⁻ ion (Fe1-Cl2 = 2.313 Å; Fe2-Cl1 = 2.301 Å) and one terminal MeOH ligand (Fe1-O5A = 2.097 Å; Fe2-O6A = 2.093 Å). The intra-molecular Fe1 \cdots Fe1', Fe1 \cdots Fe2 and Fe2 \cdots Fe2' distances are (Å): 4.043, 3.581 and 4.152. Interestingly, and despite huge efforts, no other ferric cages were obtained with *or* without the inclusion of co-ligands during our synthetic investigations with 3,5-di-*tert*-butyl-salicylaldoxime (L₂H₂). This may tentatively be attributed to the steric nature of the 3,5-di-*tert*-butyl-salicylaldoxime ligand.

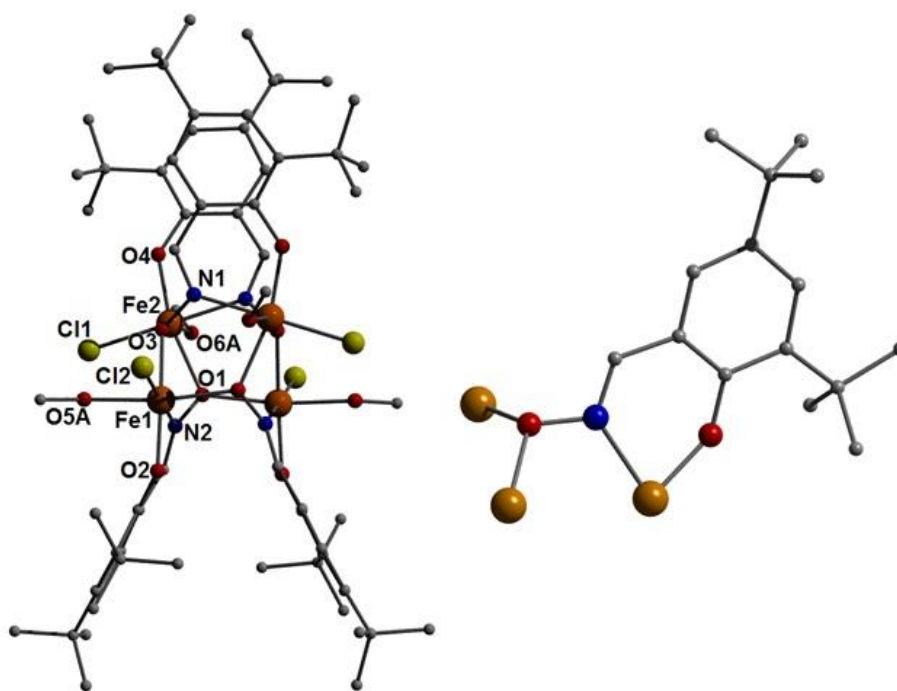


Figure 4 (left) Crystal structure of **3**. (right) The $\eta^1:\eta^1:\eta^2:\mu_3$ -bonding mode demonstrated by the 3,5-di-*tert*-butyl salicyldoxime (L_2^-) ligands in **3**. Colour code as used previously in the text (yellow = Cl). Hydrogen atoms have been omitted for clarity.

Intra-molecular interactions are observed in **3** in the form of rather long π - π interactions ($[C_2-C_7]_{\text{centroid}} \cdots [C_2'-C_7']_{\text{centroid}} = 4.587 \text{ \AA}$) and hydrogen bonding between the terminal Cl^- ligands (Cl1) and juxtaposed terminal MeOH ligands ($\text{Cl1} \cdots \text{H5A}(\text{O5A}) = 2.266 \text{ \AA}$). The $\{\text{Fe}_4\}$ units in **3** pack in a brickwork motif along the *ab* cell plane. These 2D sheets then stack in an offset parallel arrangement along the *c* direction of the unit cell (Fig. 5). The individual $\{\text{Fe}_4\}$ moieties are connected through a combination of inter-molecular C-H \cdots π exchanges (i.e. $\text{C31}(\text{H31B}) \cdots [C_{17}-C_{22}]_{\text{centroid}} = 2.888 \text{ \AA}$ and $\text{C32}(\text{H32B}) \cdots [C_2-C_7]_{\text{centroid}} = 3.174 \text{ \AA}$) and H-bonding interactions between the terminal Cl^- ions (Cl1) and methyl protons belonging to *tert*-butyl groups of adjacent L_2^{2-} ligands ($\text{Cl1} \cdots \text{H29}(\text{C29}) = 2.911 \text{ \AA}$).

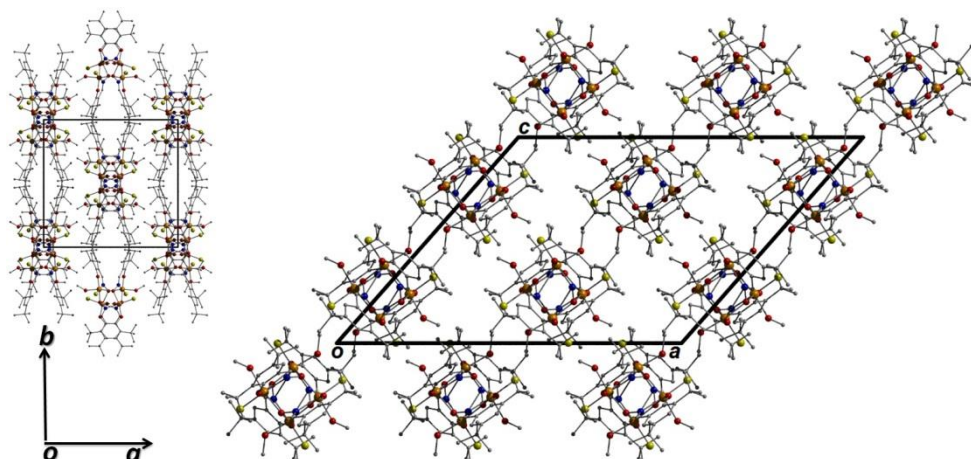


Figure 5 Packing observed in the crystal structure of **3** as viewed along the *c* (left) and *b* (right) axes of the unit cell. Hydrogen atoms have been omitted for clarity. Colour code as used previously in the text.

Table 1 Single crystal X-ray diffraction data collected on complexes **1-3**

	1	2	3
Formula ^a	C ₁₄₈ H ₁₀₈ N ₁₀ O ₂₈ Fe ₆	C ₁₈₈ H ₁₂₈ N ₁₀ O ₂₈ Fe ₆	C ₆₄ H ₁₀₀ N ₄ O ₁₂ Cl ₄ Fe ₄
<i>M</i> _w	2809.54	3310.1	1482.68
Crystal System	Triclinic	Triclinic	Monoclinic
Space group	P-1	P-1	C2/c
<i>a</i> /Å	14.0705(10)	16.5927(17)	25.946(3)
<i>b</i> /Å	15.8707(12)	17.0191(15)	18.4694(9)
<i>c</i> /Å	16.3405(12)	17.936(2)	20.669(2)
<i>α</i> ^o	108.865(7)	67.615(10)	90
<i>β</i> ^o	102.576(6)	64.944(11)	131.402(19)
<i>γ</i> ^o	94.211(6)	64.707(9)	90
<i>V</i> /Å ³	3329.0(4)	4023.1(7)	7429.5(12)
<i>Z</i>	1	1	4
<i>T</i> /K	150(2)	150(2)	150(2)
<i>λ</i> ^b /Å	0.7107	0.7107	0.7107
<i>D</i> _c /g cm ⁻³	1.401	1.366	1.326
<i>μ</i> (Mo-Kα)/mm ⁻¹	0.715	0.604	0.966
Meas./indep.(<i>R</i> _{int}) refl.	12186 / 4955 (0.112)	14712 / 3444 (0.203)	6792 / 4247 (0.070)
wR2 (all data)	0.2563	0.4281	0.1575
<i>R</i> 1 ^{d,e}	0.0936	0.1285	0.0587
Goodness of fit on <i>F</i> ²	0.985	0.944	1.036

^a Includes guest molecules. ^b Mo-Kα radiation, graphite monochromator. ^c wR2 = [Σw(|*F*_o² - |*F*_c²||²) / Σw|*F*_c²|²]^{1/2}. ^d For observed data. ^e *R*1 = Σ||*F*_o - |*F*_c|| / Σ|*F*_o|.

Table 2 Equivalent Spin Hamiltonian parameters obtained from **3** and its previously reported analogue.

Complex	J_1 (cm ⁻¹)	J_2 (cm ⁻¹)	g	Ground Spin State (S)	Ref
3	-16.0	-2.0	2.00	0	This work
[Fe ₄ (Me-sao) ₄ (Me-saoH) ₄]*	-12.4	-5.5	2.01	0	7

(* Me-saoH₂ = 2'-hydroxyacetophenone oxime)

Infra-red spectroscopic studies were carried out on air dried crystalline samples of **1-3**. Weak IR bands were observed in the 1555-1597 cm⁻¹ region of the spectra and are attributed to multiple aromatic ν (C=C) stretching vibrations [19]. The multiple bands centred on the 1578-1616 cm⁻¹ region of the spectra comprise indistinguishable ν (CO) carboxylate and ν (C=N) oxime stretching modes, as observed elsewhere [20]. Attempts at assigning the ν (N-O) oxime stretching modes in **1-3** were severely hampered by the significant spectral overlap in the 900-1150 cm⁻¹ region of the IR spectra. Previous reports on ligating aromatic oximes have documented ν (N-O) stretching IR bands in the ~1050-1250 cm⁻¹ spectral range and so should be considered here [21]. Quenching due to Fe(III) ligation in complexes **1** and **2** rendered all solid state fluorescence studies fruitless.

3.1 Magnetic susceptibility studies

Magnetic susceptibility (χ_M) measurements were carried out on powdered polycrystalline samples of **1** and **3** in the 300-5 K temperature range, in an applied dc field of 0.1 T (Fig. 7). The room temperature $\chi_M T$ values of 6.38 (**1**) and 9.54 (**3**) cm³ mol⁻¹ K are significantly lower than expected for six and four non interacting Fe(III) ions (26.25 (**1**) and 17.5 (**3**) cm³ mol⁻¹ K, assuming $g = 2.0$), respectively. Such observations are indicative of dominant antiferromagnetic interactions between the Fe(III) ions in both complexes. For **1** the $\chi_M T$ product decreases gradually with decreasing temperature, before a steeper decline is witnessed below approximately 50 K, reaching a minimum value of 1.46 cm³ mol⁻¹ K at 5 K. Fitting of the experimental data for (**1**) required use of the 3-J model (J_1 mediated by carboxylate and oxide; J_2 by carboxylate, oxide and oxime; and J_3 by alkoxide) described in Figure 6 and equation (1), affording the best-fit parameters $J_1 = -69.35$ cm⁻¹, $J_2 = -41.66$ cm⁻¹ and $J_3 = -0.32$ cm⁻¹, with g fixed to $g = 2.00$, resulting in a $S = 0$ ground state. Such values are consistent with those obtained from previously reported analogues [9a].

$$\text{Eqn. (1): } \hat{H} = 2J_1(\hat{S}_1 \cdot \hat{S}_2 + \hat{S}_2 \cdot \hat{S}_3 + \hat{S}_1' \cdot \hat{S}_2' + \hat{S}_2' \cdot \hat{S}_3') - 2J_2(\hat{S}_1 \cdot \hat{S}_3 + \hat{S}_1' \cdot \hat{S}_3') - 2J_3(\hat{S}_1 \cdot \hat{S}_3' + \hat{S}_1' \cdot \hat{S}_3 + \hat{S}_3 \cdot \hat{S}_3')$$

$$\text{Eqn. (2): } \hat{H} = 2J_1(\hat{S}_1 \cdot \hat{S}_1' + \hat{S}_2 \cdot \hat{S}_2') - 2J_2(\hat{S}_1 \cdot \hat{S}_2 + \hat{S}_1 \cdot \hat{S}_2' + \hat{S}_1' \cdot \hat{S}_2 + \hat{S}_1' \cdot \hat{S}_2')$$

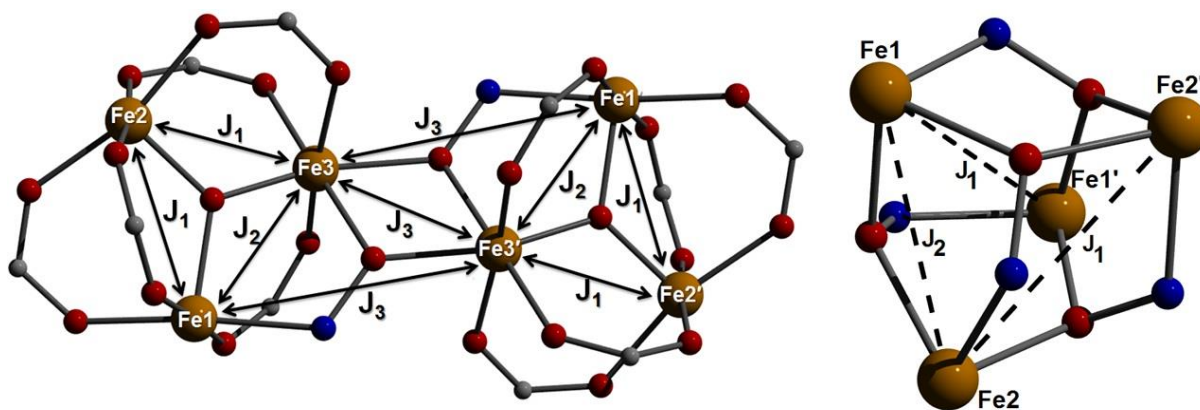


Figure 6 Schematic of the models used to fit the magnetic susceptibility data of complex **1** (left) and complex **2** (right). *Note:* for clarity not all magnetic exchange pathways have been labelled. See main text for details.

The $\chi_{\text{M}}T$ vs. T plot for complex **3** is also indicative of dominant antiferromagnetic exchange and a diamagnetic ground state (Fig. 7). Fitting of the magnetic susceptibility data employed the 2J model of equation 2, illustrated in Fig. 6, in which J_1 represents the Fe1 \cdots Fe1' and Fe2 \cdots Fe2' vectors comprising 2 \times Fe-N-O-Fe oxime bridging pathways, and J_2 represents the Fe1 \cdots Fe2, Fe1' \cdots Fe2', Fe1 \cdots Fe2' and Fe1' \cdots Fe2 vectors comprising 1 \times Fe-N-O-Fe and 1 \times Fe-O-Fe magnetic exchange pathway (Fig. 6). The best fit afforded $J_1 = -16.0 \text{ cm}^{-1}$ and $J_2 = -2.0 \text{ cm}^{-1}$, with g fixed to $g = 2.00$, which are comparable to the parameters fitted from the structurally similar $[\text{Fe}_4(\text{Me-sao})_4(\text{Me-saoH})_4]$ (where Me-saoH₂ = 2'-hydroxyacetophenone oxime) (Table 2) [7].

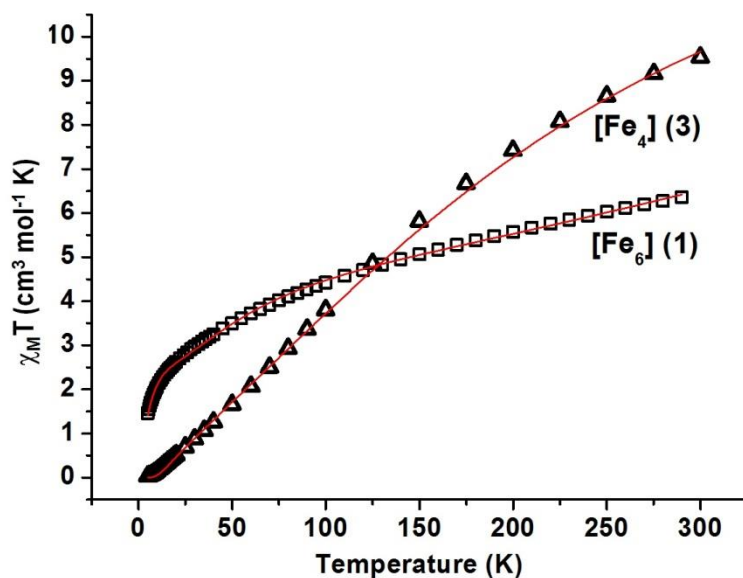


Figure 7 Plot of $\chi_{\text{M}}T$ vs T for complexes **1** (\square) and **3** (Δ). The red lines represent the best-fit of the experimental data. See main text for details.

4. Concluding Remarks

We have described the synthesis of two hexanuclear ferric cages $[\text{Fe}(\text{III})_6\text{O}_2(\text{L}_1)_2(\text{O}_2\text{C}-\text{C}_{10}\text{H}_8)_{10}(\text{H}_2\text{O})_2] \cdot 8\text{MeCN}$ (**1**) and $[\text{Fe}(\text{III})_6\text{O}_2(\text{L}_1)_2(\text{O}_2\text{C}-\text{C}_{14}\text{H}_{10})_{10}(\text{H}_2\text{O})_2] \cdot 8\text{MeCN}$ (**2**). The core topologies in **1** and **2** are derived from the fusion of two $\{\text{Fe}(\text{III})_3\text{O}(\text{O}_2\text{CR})_5\}^{2+}$ triangular units ($\text{R} = \text{C}_{10}\text{H}_8$; $\text{C}_{12}\text{H}_{10}$) and are encased by an organic sheath provided by the combination of extremely bulky polyphenolic oxime and carboxylate ligands. The bulky 3,5-di-*tert*-Butyl-salicylaldoxime (L_2H_2) ligand led to the formation of the distorted cubane complex $[\text{Fe}(\text{III})_4(\text{L}_2)_4(\text{MeOH})_4(\text{Cl})_4]$ (**3**). Magnetic susceptibility data obtained for **1** and **3** revealed relatively strong antiferromagnetic exchange between nearest neighbours in both cases, leading to diamagnetic ground states. Best fit spin Hamiltonian parameters were $J_1 = -69.35 \text{ cm}^{-1}$, $J_2 = -41.66 \text{ cm}^{-1}$, $J_3 = -0.23 \text{ cm}^{-1}$ (**1**) and $J_1 = -16.0 \text{ cm}^{-1}$, $J_2 = -2.0 \text{ cm}^{-1}$ (**3**).

Acknowledgements

LFJ wishes to thank the Irish Research Council for Science and Technology (IRCSET Embark Program (EH)) for their support. EKB thanks the EPSRC.

References

- [1] A. M. Wilson, P. J. Bailey, P. A. Tasker, J. R. Turkington, R. A. Grant and J. B. Love. *Chem. Soc. Rev.*, 43, (2014), 123-134. (b) B. K. Tait, K. E. Mdlalose and I. Taljaard. *Hydrometallurgy*. 38, (1995), 1-6.
- [2] R. S. Forgan, B. D. Roach, P. A. Wood, F. J. White, J. Campbell, D. N. Hendrickson, E. Kamenetsky, F. E. McAllister, S. Parsons, E. Pidcock, P. Richardson, R. M. Swart and P. A. Tasker. *Inorg. Chem.*, 50, (2001), 4515-4522.
- [3] *For a comprehensive review on the coordination chemistry of phenolic oximes see:* A. G. Smith, P. A. Tasker and D. J. White. *Coord. Chem. Rev.*, 241, (2003), 61-85.
- [4] *For a comprehensive review on the coordination chemistry of pyridyl oximes see:* C. J. Milios, T. C. Stamatatos and S. P. Perlepes. *Polyhedron*. 25, (2006), 134-194.
- [5] R. Inglis, C. Milios, L. F. Jones, S. Piligkos, E. K. Brechin. *Chem. Commun.*, (Feature Article), 48, (2011), 181-190.
- [6] R. Inglis, L. F. Jones, C. J. Milios, S. Datta, A. Collins, S. Parsons, W. Wernsdorfer, S. Hill, S. P. Perlepes, S. Piligkos, E. K. Brechin. *Dalton Trans.*, (2009), 3403-3412.
- [7] I. A. Gass, C. J. Milios, A. Collins, F. J. White, L. Budd, S. Parsons, M. Murrie, S. P. Perlepes and E. K. Brechin. *Dalton Trans.*, (2008), 2043-2053.
- [8] K. Mason, I. A. Gass, F. J. White, G. S. Papaefstathiou, E. K. Brechin and P. A. Tasker. *Dalton Trans.*, 40, (2011), 2875-2881.
- [9] (a) C. P. Raptopoulou, A. K. Boudalis, Y. Sanakis, V. Psycharis, J. M. Clement-Juan, M. Fardis, G. Diamantopoulos and G. Papavassiliou. *Inorg. Chem.*, 45, (2006), 2317-2326. (b) K. Mason, I. A. Gass, S. Parsons, A. Collins, F. J. White, A. M. Z. Slavin, E. K. Brechin and P. A. Tasker. *Dalton Trans.*, 39, (2010), 2727-2734
- [10] *For examples of Fe-salicyldoxime complexation see:* (a) I. A. Gass, C. J. Milios, A. G. Whittaker, F. P. A. Fabiani, S. Parsons, M. Murrie, S. P. Perlepes and E. K. Brechin. *Inorg. Chem.*, 45, (2006), 5281-5283. (b) P. Chaudhuri, E. Rentschler, F. Birkelbach, C. Krebs, E. Bill, T. Weyhermüller and U. Flörke. *Eur. J. Inorg. Chem.*, (2003), 541-555. (c) C. Nazari Verani, E. Bothe, D. Burdinski, T. Weyhermüller, U. Flörke and P. Chaudhuri. *Eur. J. Inorg. Chem.*, (2001), 2161-2169. (d) J. M. Thorpe, R. L. Beddoes, D. Collison, C. D. Garner, M. Helliwell, J. M., Holmes and P. A. Tasker. *Angew. Chem. Int. Ed.*, 38(8), (1999), 1119-1121. (e) E. Bill, C. Krebs, M. Winter, M. Gerdan, A. X. Trautwein, U. Flörke, H.-J. Haupt and P. Chaudhuri. *Chem. Eur. J.*, 3, (1997), 193-201.
- [11] G. M. Sheldrick, *Acta. Crystallogr., Sect. A: Found. Crystallogr.*, A46, (1990), 467.

- [12] G. M. Sheldrick, SHELXL-97, A computer programme for crystal structure determination, University of Gottingen, 1997.
- [13] P. McArdle, P. Daly and D. Cunningham, *J. Appl. Crystallogr.*, 35, (2002), 378.
- [14] R. Dunsten and T. A. Henry. *J. Chem. Soc. Trans.*, 75, (1899), 66.
- [15] C. Canada-Vilalta, T. A. O'Brien, E. K. Brechin, M. Pink, E. R. Davidson and G. Christou. *Inorg. Chem.*, 43, (2004), 5505-5521.
- [16] C. Canada-Vilalta, E. Rumberger, E. K. Brechin, W. Wernsdorfer, K. Folting, E. R. Davidson, D. N. Hendrickson and G. Christou. *J. Chem. Soc. Dalton. Trans.*, (2002), 4005-4010.
- [17] For an extensive family comprising the $\{\text{Fe}_6\text{O}_2(\text{OH})_2\}^{12+}$ core using a plethora of amino alcohol ligands see: C. Papatriantafyllopoulou, C. M. Kizas, M. J. Manos, A. Boudalis and A. J. Tasiopoulos. *Polyhedron*. 64, (2013), 218.
- [18] Mehrotra, R. C.; Bohra, R. *Metal Carboxylates*; Academic Press: London, (1983); Chapter 3.2.3. (b) R. D. Cannon and R. P. White. *Prog. Inorg. Chem.* 36, (1988), 195.
- [19] G. Socrates. *Infra-Red and Raman Characteristic Group Frequencies*. (2004) Wiley VCH Publishing.
- [20] F. Birkelbach, M. Winter, U. Flörke, H.-J. Haupt, C. Butzlaff, M. Lengen, E. Bill, A. X. Trautwein, K. Wieghardt and P. Chaudhuri. *Inorg. Chem.*, 33, (1994), 3990-4001.
- [21] (a) C. Papatriantafyllopoulou, G. Aromi, A. J. Tasiopoulos, V. Nastopulos, C. P. Raptopoulou, S. J. Teat, A. Escuer and S. P. Perlepes. *Eur. J. Inorg. Chem.*, (2007), 2761-2774. (b) T. Weyhermüller, R. Wagner, S. Khandra and P. Chaudhuri. *Dalton Trans.*, (2005), 2539-2546. (c) P. Chaudhuri, M. Winter, U. Flörke and H.-J. Haupt. *Inorg. Chim. Acta.*, 232, (1995), 125-130.

Graphical Abstract:

Bulking Up: Sterically demanding oxime and carboxylate ligands combine to aid the self-assembly of hexanuclear $[\text{Fe}_6]$ cages. Magnetic susceptibility measurements reveal dominant antiferromagnetic exchange between the Fe(III) centres.

